Phase Contrast MRI Measurements of Net Cerebrospinal Fluid Flow Through the Cerebral Aqueduct Are Confounded by Respiration

Jolanda M. Spijkerman, MSc,[1]* Lennart J. Geurts, MSc,[1] Jeroen C.W. Siero, PhD,[1,2] Jeroen Hendrikse, MD, PhD,[1] Peter R. Luijten, PhD,[1] and Jaco J.M. Zwanenburg, PhD[1]

Background: Net cerebrospinal fluid (CSF) flow through the cerebral aqueduct may serve as a marker of CSF production in the lateral ventricles, and changes that occur with aging and in disease.
Purpose: To investigate the confounding influence of the respiratory cycle on net CSF flow and stroke volume measurements.
Study Type: Cross-sectional study.
Subjects: Twelve young, healthy subjects (seven male, age range 19–39 years, average age 28.3 years).
Field Strength/Sequence: Phase contrast MRI (PC-MRI) measurements were performed at 7T, with and without respiratory gating on expiration and on inspiration. All measurements were repeated.
Assessment: Net CSF flow and stroke volume in the aqueduct, over the cardiac cycle, was determined.
Statistical Tests: Repeatability was determined using the intraclass correlation coefficient (ICC) and linear regression analysis between the repeated measurements. Repeated measures analysis of variance (ANOVA) was performed to compare the measurements during inspiration/expiration/no gating. Linear regression analysis was performed between the net CSF flow difference (inspiration minus expiration) and stroke volume.
Results: Net CSF flow (average ± standard deviation) was 0.64 ± 0.32 mL/min (caudal) during expiration, 0.12 ± 0.49 mL/min (cranial) during inspiration, and 0.31 ± 0.18 mL/min (caudal) without respiratory gating. Respiratory gating did not affect stroke volume measurements (41 ± 18, 42 ± 19, 42 ± 19 μL/cycle for expiration, no respiratory gating and inspiration, respectively). Repeatability was best during inspiration (ICC = 0.88/0.56/–0.31 for gating on inspiration/expiration/no gating). A positive association was found between average stroke volume and net flow difference between inspiration and expiration (R = 0.678/0.605, P = 0.015/0.037 for the first/second repeated measurement).
Data Conclusion: Measured net CSF flow is confounded by respiration effects. Therefore, net CSF flow measurements with PC-MRI cannot in isolation be directly linked to CSF production.
Level of Evidence: 1
Technical Efficacy: Stage 2

J. MAGN. RESON. IMAGING 2019;49:433–444.

Cerebrospinal fluid (CSF) plays an important role in maintaining homeostasis and in the clearance system of the brain.[1,2] With aging, CSF production and CSF flow decline,[3,4] which may be due to age-related cognitive decline.[5,6] Also, in normal pressure hydrocephalus CSF flow is altered.[7] Therefore, noninvasive measurements of CSF production in combination with advanced brain imaging may provide a useful tool to study the role of CSF changes in aging and disease. CSF net flow through the cerebral aqueduct (aqueduct of Sylvius) over the cardiac cycle can

View this article online at wileyonlinelibrary.com. DOI: 10.1002/jmri.26181

Received Feb 6, 2018, Accepted for publication Apr 19, 2018.

*Address reprint requests to: J.M.S., Department of Radiology, University Medical Center Utrecht, 3508 GA Utrecht, The Netherlands. E-mail: j.m.spijkerman-4@umcutrecht.nl

From the [1]Department of Radiology, University Medical Center Utrecht, Utrecht, Netherlands; and [2]Spinoza Center for Neuroimaging, Amsterdam, Netherlands

This is an open access article under the terms of the Creative Commons Attribution-NonCommercial License, which permits use, distribution and reproduction in any medium, provided the original work is properly cited and is not used for commercial purposes.

© 2018 The Authors *Journal of Magnetic Resonance Imaging* published by Wiley Periodicals, Inc. on behalf of International Society for Magnetic Resonance in Medicine

potentially serve as a measure for CSF production in the lateral ventricles by the choroid plexus, and can be measured using phase-contrast magnetic resonance imaging (PC-MRI).[8–12] PC-MRI can be acquired in ~2 minutes of imaging time[4,11]; hence, the resulting CSF flow waveform is the average of many cardiac cycles.

PC-MRI measurements of net CSF flow over the cardiac cycle rely on the assumption that relatively large CSF displacements due to the respiratory cycle[13–16] average out over the acquisition time of the measurements.[10] Although this seems a reasonable assumption, given the relatively long acquisition time compared to the duration of the respiratory cycle, respiration may be a stronger confounder in the PC-MRI measurements of net CSF flow than expected. In fact, reversed net CSF flow (in cranial direction) has also incidentally been observed in healthy subjects in several studies.[17,18] Possibly incomplete averaging of respiratory effects contributed to these cases of reversed net CSF flow.

The main goals of this work were to determine the net CSF flow over the cardiac cycle through the cerebral aqueduct, and to investigate whether the net CSF flow measurements are confounded by respiratory-induced CSF motion. We hypothesized that the incidentally observed reversed net CSF flows may be due to respiratory effects. Our secondary goals were, first, to determine the repeatability of the measurements and, second, to compare CSF stroke volume (cardiac-induced pulsatility) with the size of the confounding effect from respiration (as a measure for respiration-induced CSF pulsatility).

Materials and Methods

Experimental Design

Twelve young, healthy volunteers (seven male, age range 19–39 years, average age 28.3 years) participated in this study. Informed consent was given in accordance to the Institutional Review Board of the University Medical Center Utrecht (Utrecht, The Netherlands). To achieve high signal-to-noise ratio (SNR) and good spatial resolution, which minimizes partial volume, the measurements were performed at 7T MRI (Philips Healthcare, Best, The Netherlands) using a volume transmit coil and a 32-channel receive coil (Nova Medical, Wilmington, MA). Physiology was recorded using vendor-supplied equipment: the peripheral pulse unit (PPU) was used for cardiac gating, and the respiratory belt was used for respiratory gating. Since the circadian rhythm has been reported to influence net CSF flow,[18] all measurements were conducted between 8:00 and 10:00 AM. PC-MRI measurements were performed in the cerebral aqueduct with encoding velocity (v_{enc}) 15 cm/s. A single slice was acquired, with acquired resolution 0.45 × 0.45 × 3 mm^3 reconstructed to 0.25 × 0.25 × 3 mm^3, field of view (FOV) 190 × 248 × 300 mm^3, and 36–45 frames were reconstructed per cardiac cycle, depending on the heart rate of the volunteer. Other parameters were: repetition time / echo time (TR/TE) 12/5.9 msec, R-R window 15%/25%, 2 k-lines per cardiac cycle with alternating positive and negative flow encoding for background phase error removal (yielding an acquired temporal resolution of 4*TR = 48 msec), bandwidth 375.2 Hz/pixel, flip angle 12°, and SENSE factor 2. Retrospective cardiac gating was performed. A whole-brain 3D T_1-weighted TFE scan (resolution 1 mm isotropic, FOV 190 × 248 × 300 mm^3, TR/TE 4.2/2.0 msec, inversion recovery time 1281 msec, TR between inversion pulses 3000 msec, flip angle 7°, SENSE factor 2, scan time 2:00 min) and a whole-brain T_2-weighted 3D balanced gradient echo scan (resolution 0.6 mm isotropic, FOV 192 × 221 × 250 mm^3, TR/TE 5.0/1.9 msec [partial echo], flip angle 30°, SENSE factor 2.1, scan time 1:44 min) were acquired for planning of the PC-MRI scan, as illustrated in Fig. 1A,B. The volunteers were instructed to perform calm abdominal breathing. The PC-MRI measurements were performed for two different forms of respiratory gating: 1) respiratory gating on expiration and 2) respiratory gating on inspiration, resulting in image acquisition only during expiration or inspiration. Respiratory gating on expiration was available in the vendor-supplied scanner software; this was extended to also allow for gating on inspiration. This was compared with no respiratory gating, which can be regarded as the current common practice. Each protocol was repeated (without repositioning of the subject) to allow assessment of repeatability of the potential effect of respiration: apart from differences in the respiratory and cardiac traces, there were no variations between the scans. Scan time per scan varied between 1:28–1:52 minutes without respiratory gating, and between 4:26–5:38 minutes with respiratory gating, depending on the heart rate of the volunteer.

Data Processing

Background correction was performed with a method previously developed for blood flow velocity quantification in small perforating arteries,[19] in addition to the background velocity correction provided by the vendor. Mean background phase was determined by applying a median filter (kernel size 15 × 15 mm^2) to the mean of all phase images over the cardiac cycle. This mean background phase was then subtracted from all phase images over the cardiac cycle.

Thereafter a region-of-interest (ROI) of the brain stem was drawn manually on the magnitude image of each scan (Fig. 1C) to facilitate automatic detection of the aqueduct area. Phase unwrapping was performed within this ROI using Goldstein's method,[20] in all scans that showed phase wrapping at any timepoint in the cardiac cycle.

Subsequently, the cerebral aqueduct was automatically determined within the brainstem ROI, by selecting the voxels with significant signal intensity relative to the background, using the magnitude images. The aqueduct mask was determined in two steps. First, the mean background magnitude was obtained by median filtering the mean magnitude image (kernel size 15 × 15 mm^2). Second, the standard deviation (SD) of the real and imaginary parts of the signal over the cardiac cycle was determined pixel-by-pixel. The root-mean-square of the real and imaginary SD was median filtered (kernel size 15 × 15 mm^2) and used as a map of the noise background. The background signal was assumed to be stable over the cardiac cycle; therefore, signal variation over the cardiac cycle was regarded as noise. One aqueduct mask was determined for all phases over the cardiac cycle, assuming that the

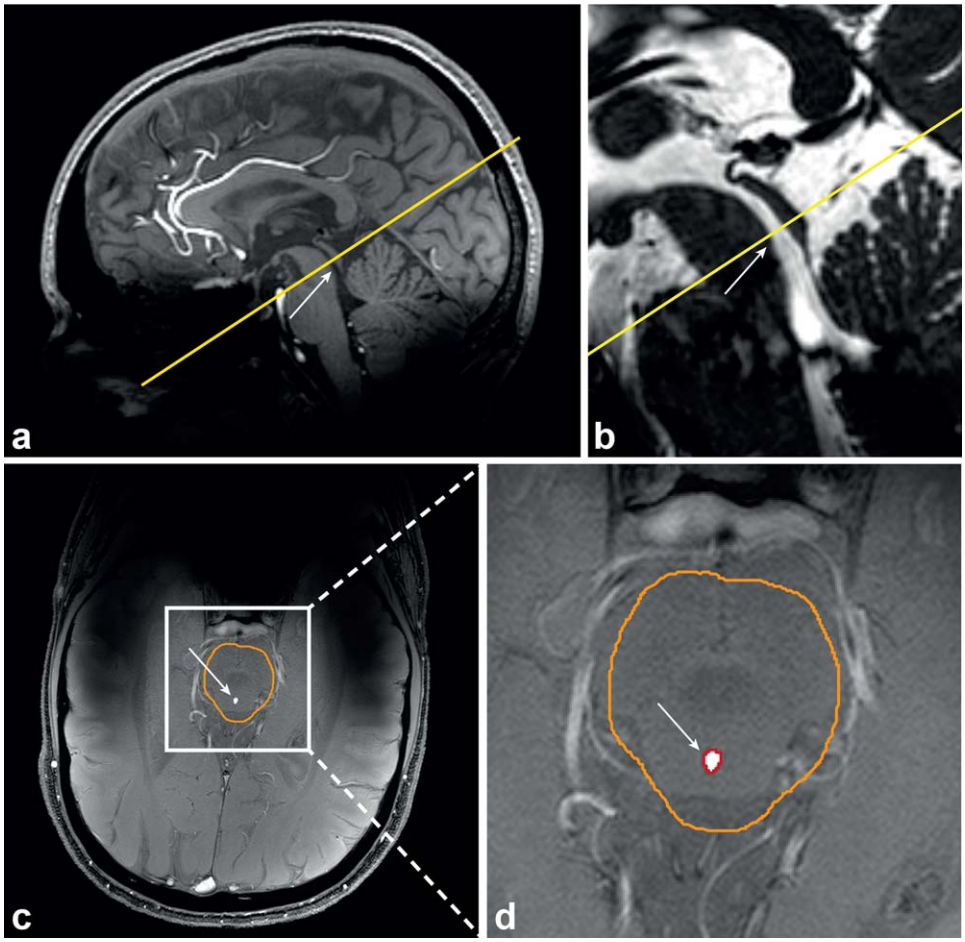

FIGURE 1: Slice planning of the PC-MRI scan (single slice, yellow) for Volunteer 5, relative to a whole-brain 3D T_1-weighted TFE scan (A) and a whole-brain T_2-weighted 3D balanced gradient echo scan (B), the corresponding, manually drawn, brain stem ROI (orange) in the magnitude image (C), and the automatically determined aqueduct ROI (red) (D). The cerebral aqueduct is indicated by the white arrow.

diameter variation was well below the image resolution. The aqueduct mask was defined as all voxels with a signal intensity significantly above the background magnitude, and were automatically determined using the estimated background noise map and significance level $P < 0.01$.[19] An example of the resulting aqueduct mask is shown in Fig. 1D.

Finally, the average velocity curve of the aqueduct ROI was determined. The net velocity over the cardiac cycle was determined by integrating the average CSF velocity curve over the cardiac cycle. To obtain the net CSF flow over the cardiac cycle the net velocity was multiplied by the aqueduct area. By convention in this article, positive flows are in the cranial direction, negative flows are in the caudal direction. To assess the net flow profiles in the aqueduct, for all subjects the net velocity per voxel was plotted. Furthermore, stroke volumes were determined by averaging the (absolute) systolic (caudal) and diastolic (cranial) flow volumes through the aqueduct over the cardiac cycle, for each measurement.

Statistical Analysis

As a measure for the repeatability of the net CSF flow and stroke volume measurements, the difference and absolute difference in net CSF flow between the repeated measurements were determined for each subject. Also, the intraclass correlation coefficient (ICC) was determined, and linear regression analysis between the first (independent variable) and second (dependent variable) was performed.

To visually compare the CSF flow for the different respiratory conditions, the mean normalized CSF flow curves were plotted for each respiratory condition. First, the CSF flow curves were interpolated to 100 timepoints (0–100% of the cardiac cycle). Subsequently, all flow curves were normalized relative to the absolute maximal observed flow in any of the six measurements (three respiratory conditions, each repeated), and the average flow curve for each respiratory condition was determined. Finally, the mean ± standard error of the mean (SEM) flow curve of all volunteers were determined for each respiratory condition.

To compare the different respiratory conditions, boxplots were made for the average measured net CSF flow per subject during inspiration gating, expiration gating, and without respiratory gating. Repeated measures analysis of variance (ANOVA) was performed to compare the net CSF flows and stroke volumes during inspiration gating, expiration gating, and without respiratory gating, for the first and the second measurements separately. A significance level of $P < 0.05$ was used, and Bonferroni correction was applied for the pairwise comparisons (three tests).

To explore the relation between CSF pulsatility (stroke volume) and the influence of respiration phase on net CSF flow,

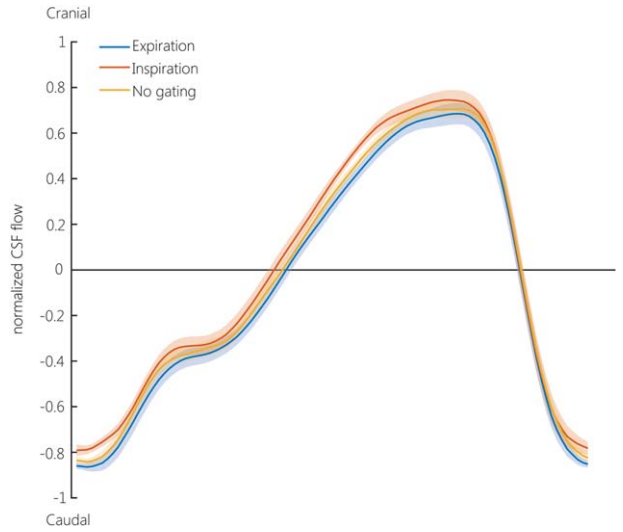

FIGURE 2: Average normalized CSF velocity in the aqueduct over the cardiac cycle, averaged over both repeated measurements and all subjects, during expiration (blue), inspiration (orange), and no gating (yellow). The CSF flow curves were interpolated (using cubic interpolation with the MatLab function interp1) to 100 timepoints (0–100% of the cardiac cycle). As triggering was performed using a peripheral pulse oximeter, the cardiac cycle starts around peak-systole. The cardiac cycle duration varied between 857–1090 msec. The line represents the average CSF velocity, the transparent band represents the SEM. The normalization was performed per subject, by dividing by the maximum absolute velocity of any of the six measurements (three respiratory conditions, each measured twice).

linear regression analyses were performed between the net CSF flow difference for inspiration minus expiration (dependent variable) and the average stroke volume of inspiration and expiration (independent variable), for the first and second measurements separately. A significance level of $P < 0.05$ was used.

Data processing was performed with MatLab (v. 2017A, MathWorks, Natick, MA). Statistical analyses were performed with IBM SPSS (v. 24, Armonk, NY).

Results

Scans were successfully completed in all volunteers. In 10 scans, of three subjects, phase unwrapping was performed. The size of the automatically acquired aqueduct ROIs varied between 1.3–5.8 mm^2. No difference in background correction was found between gating on inspiration, expiration, or no respiratory gating (data not shown). The maximum CSF velocities varied between 3.4–16.7, 2.8–13.0, 3.1–15.7 cm/s, during inspiration gating, expiration gating, and without respiratory gating, respectively. No (inverse) correlation was found between the aqueduct area and the maximum CSF velocity. No correlation was found between the cardiac frequency and the net CSF flow or between the cardiac frequency and the stroke volume. Between the various CSF flow scans, the cardiac frequency ranged between 97 and 105% of the average cardiac frequency for each subject (percentages averaged over all volunteers, min/max observed difference was 95% and 109%). The respiratory frequencies ranged between 0.16–0.32 Hz.

CSF Flow and Stroke Volume Relative to the Respiratory Phase

Figure 2 shows the mean ± SEM normalized CSF flow in the aqueduct over the cardiac cycle during expiration gating, inspiration gating, and without respiratory gating in all volunteers and for both repeated measurements. The CSF flow curve for the inspiration gated measurements lies consistently above the curve for expiration gated measurements, and the curve for no respiratory gating lies in between the curves for inspiration and expiration. Individual CSF flow curves during inspiration and expiration gating for the first measurement show generally the same pattern, and are shown in Fig. 3.

Figure 4A shows the average net CSF flow per subject during inspiration gating, expiration gating, without respiratory gating. During expiration the largest caudal net CSF flows were found; during inspiration the largest cranial net CSF flows were found. The net CSF flows measured without respiratory gating are in between the net CSF flows measured during expiration and inspiration. Figure 4B shows the average net CSF flow during the different respiratory conditions per subject. In 9 out of 12 subjects, during expiration the most caudal (negative) net flow was found, and during inspiration net flow was cranial (positive) or considerably smaller compared with expiration. For two subjects, similar caudal net CSF flows were found during expiration and inspiration. One subject showed a somewhat reversed effect, with caudal net flow during inspiration (0.35 mL/min and 0.18 mL/min for the repeated measurements, respectively) and inconsistent net flow during expiration (0.04 mL/min in the caudal direction, and 0.15 mL/min in the cranial direction for the repeated measurements, respectively).

The repeated measures ANOVA showed that overall significantly different net CSF flows were measured between the respiratory conditions (tests of within-subject effects): the resulting *P*-values were 0.001 ($F(2,11) = 9.31$) and 0.001 ($F(2,11) = 10.07$) for the first and second measurement, respectively. The pairwise comparisons showed that the difference in net CSF flow between expiration and inspiration is very similar between the repeated measurements. The resulting mean differences and the corresponding *P*-values for the pairwise comparisons are summarized in Table 1. For the stroke volumes no (significant) differences were found between the respiratory conditions: the resulting *P*-values were 0.122 ($F(2,11) = 1.52$) and 0.23 ($F(2,11) = 3.29$) for the first and second measurement, respectively.

The net CSF flow for all aqueduct voxels during expiration gating, inspiration gating, and without respiratory gating for all subjects, for the first measurement, is shown in Fig. 5. Large intersubject variation can be observed between the net CSF flow profiles over the aqueduct. The

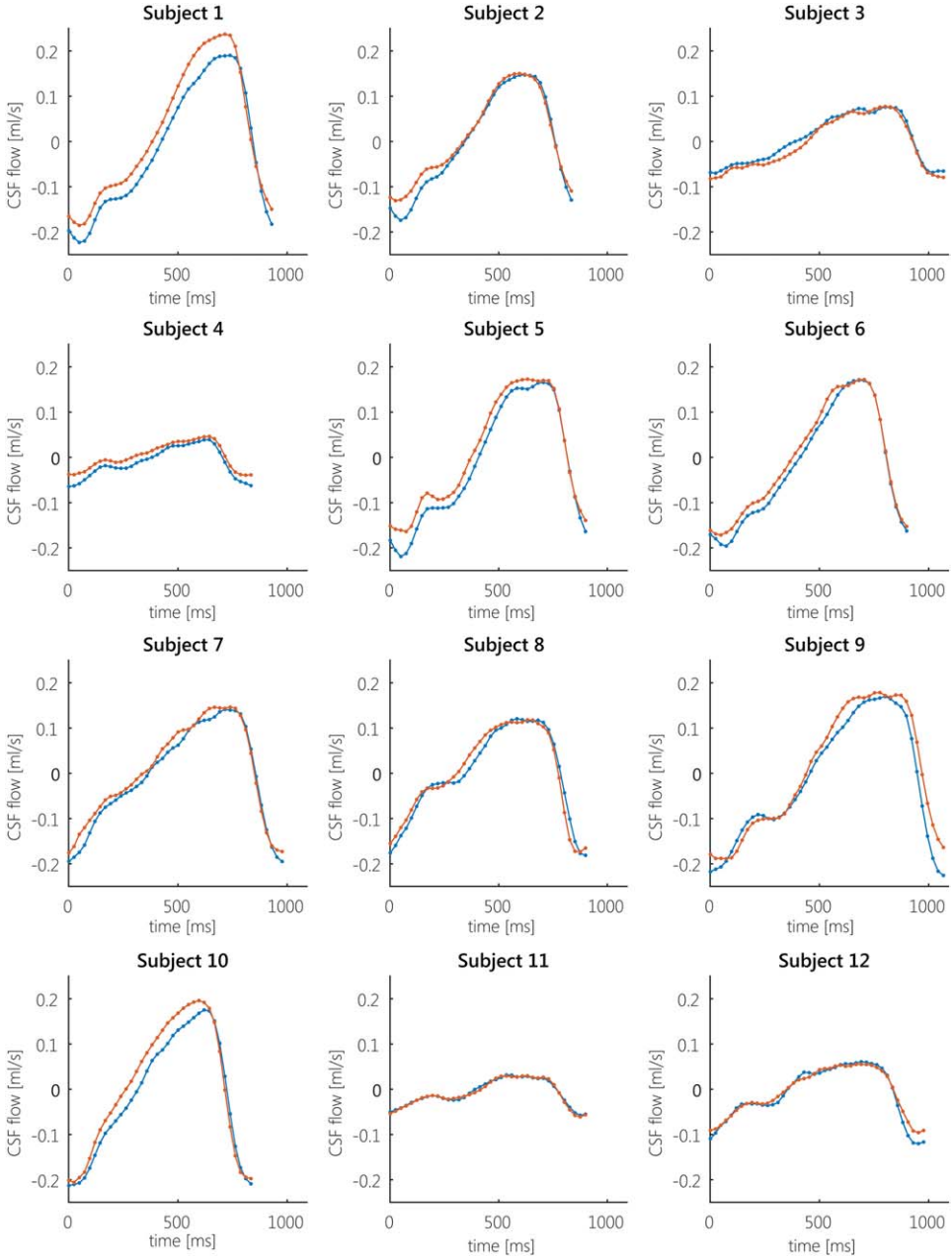

FIGURE 3: Individual CSF flow profiles during inspiration (orange) and expiration (blue) for all subjects, for the first measurement. Positive CSF flow is in cranial direction, negative CSF flow is in caudal direction. For most subjects, the CSF flow profile during inspiration is above the CSF flow profile during expiration. Subject 3 showed cranial net flow during expiration, and caudal flow during inspiration. Subjects 11 and 12 showed similar flows during inspiration and expiration.

subject-specific patterns were consistent between the various breathing gating schemes, but generally more cranial flow was observed during inspiration gating compared to expiration gating or no gating. Very similar net flow patterns were found during the second measurement (data not shown).

Repeatability of Net CSF Flow and Stroke Volume Measurements

Figure 4C shows the individual net CSF flows for each subject, for the repeated measurements. For the measurements without respiratory gating the largest within-subject variation can be observed, compared with the respiratory gated measurements. The repeatability results for the net CSF flows and stroke volumes for expiration gating, without respiratory gating, and inspiration gating are summarized in Table 2. The mean net CSF flow was negative (caudal) during expiration gating and without respiratory gating, and positive (cranial) during inspiration gating, for both measurements. The difference and absolute difference between the repeated measurements is larger without respiratory gating compared with the inspiration and expiration gated measurements. Also, the SD of the difference between the repeated measurements is largest without respiratory gating. During inspiration gating the SD of the difference between

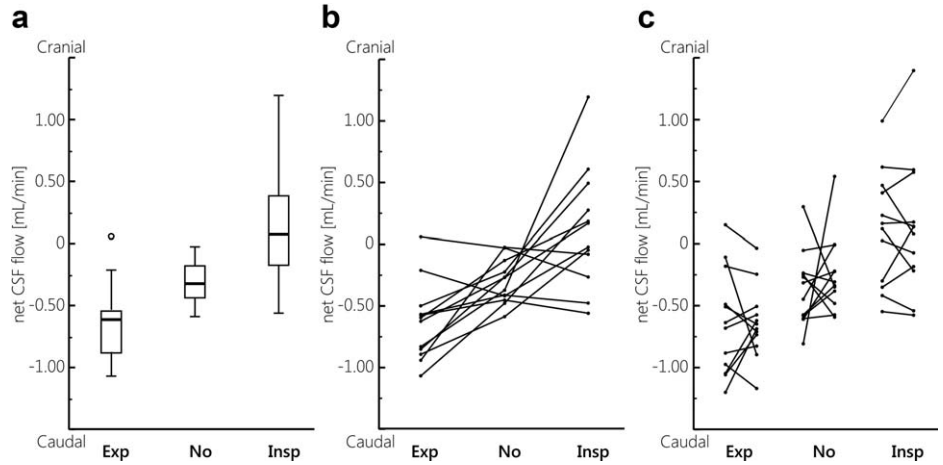

FIGURE 4: A: Boxplots showing the mean net CSF flow (over both measurements) measured in each subject, during expiration gating (Exp), no gating (No), and inspiration gating (Insp). Outliers are represented by the open circles. Except for one outlier, only negative (caudal) flows were measured during expiration, while during inspiration often positive (cranial) flows were measured. B: Mean net CSF flow measured in each subject. Generally, the net CSF flow measured without respiratory gating is in between the net CSF flows measured during expiration and inspiration. C: Net CSF flow measured in each subject during the first and second measurement.

the repeated measurements is smallest, and the ICC is largest. Without respiratory gating ICC is negative. Regression analysis resulted in significant correlations between the first and second measurement for inspiration and expiration gating, as shown in Fig. 6A–C. For the inspiration gated measurements, the regression line was approximately M2 = M1, indicating good repeatability.

For all respiratory conditions and both measurements, similar stroke volumes were measured. The difference and absolute difference in stroke volume between the repeated measurements were close to zero, the ICCs were high (minimally 0.98). Regression analysis resulted in significant correlations between the first and second measurement, as shown in Fig. 6D–F. For all respiratory conditions the regression line was approximately M2 = M1. The stroke volumes were highly repeatable, regardless of the type of respiratory gating.

Net CSF Flow Difference Relative to CSF Stroke Volume

Overall, smaller net CSF flow differences between inspiration and expiration gating were observed for the subjects who showed less pulsatile (flatter) CSF flow curves (Fig. 3); this can also be observed from the smaller difference between the CSF flow profiles during the inspiration and expiration gated measurements. Linear regression analysis confirmed this correlation between net CSF flow difference (inspiration gated minus expiration gated) (dependent variable) and stroke volume (average stroke volume of inspiration and expiration) (independent variable), as illustrated in Fig. 7: for both measurements significant, positive associations were found.

Discussion

This work investigated whether net CSF flow measurements with PC-MRI are confounded by respiratory-induced CSF motion, by performing PC-MRI measurements with various respiration conditions, using respiratory gating. The results confirmed that net CSF flow measurements are confounded by respiration: consistent caudal net CSF flow was found during expiration, while on average cranially directed net CSF flow was found during inspiration. Stroke volumes were not affected by respiratory gating. The repeatability of

TABLE 1. CSF Net Flow Differences

		Mean difference ± SEM [mL/min]	*P*-value
Measurement 1	Expiration – Inspiration	–0.75 ± 0.20	0.010*
	No gating – Expiration	–0.26 ± 0.15	0.348
	No gating – Inspiration	0.49 ± 0.17	0.045*
Measurement 2	Expiration – Inspiration	–0.76 ± 0.20	0.008*
	No gating – Expiration	–0.39 ± 0.12	0.027*
	No gating – Inspiration	0.37 ± 0.18	0.196

Net CSF flow differences (mean ± SEM). Between the respiratory gating conditions and the corresponding *P*-values, for the pairwise comparisons of the repeated measures ANOVA, for the first and the repeated net CSF flow measurements during expiration gating, inspiration gating, and without respiratory gating. Significant *P*-values are represented by the asterisk symbol.

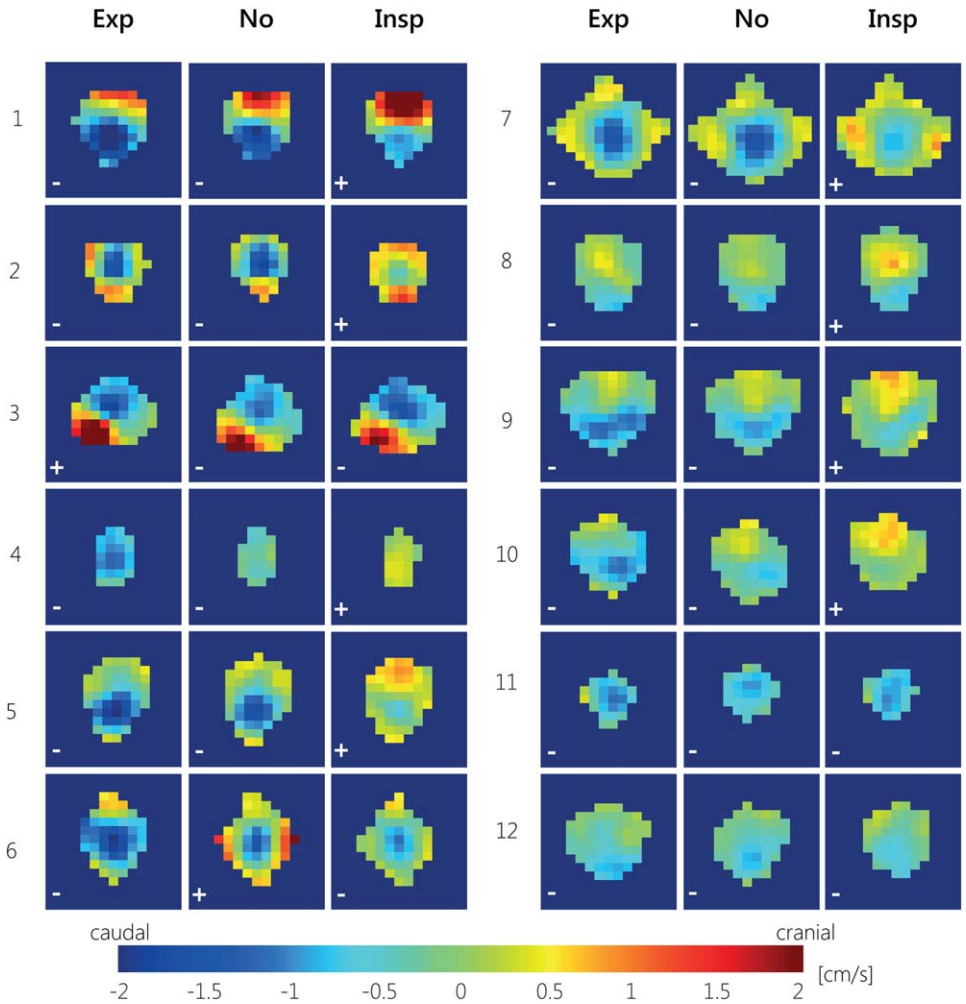

FIGURE 5: CSF net flow for all aqueduct voxels during expiration gating (Exp), inspiration gating (Insp), and without respiratory gating (No) for all 12 subjects, for the first measurement. For most subjects, during expiration gating most voxels show caudal net CSF flow, and during inspiration gating more voxels show (larger) cranial net CSF flow. The net CSF flow directions are indicated with ± symbols for cranial/caudal net CSF flow.

TABLE 2. Repeatability of Net CSF Flow and CSF Stroke Volume

	Net CSF flow [mL/min]			Stroke volume [μL/cycle]		
	Exp	**No**	**Insp**	**Exp**	**No**	**Insp**
Measurement 1 (M1)	-0.63 ± 0.42	-0.37 ± 0.30	0.12 ± 0.46	42 ± 18	43 ± 19	41 ± 18
Measurement 2 (M2)	-0.64 ± 0.29	-0.24 ± 0.31	0.13 ± 0.54	41 ± 18	42 ± 20	43 ± 20
Average: (M1+M2)/2	-0.64 ± 0.32	-0.31 ± 0.18	0.12 ± 0.49	41 ± 18	42 ± 19	42 ± 19
Difference: M1 – M2	0.003 ± 0.35	-0.13 ± 0.49	-0.01 ± 0.25	2 ± 2	0 ± 2	-1 ± 4
Absolute difference: |M1 – M2|	0.26 (0.06–0.79)	0.34 (0.03–1.35)	0.19 (0.01–0.43)	2 (0–4)	2 (0–4)	3 (0–8)
Intraclass correlation coefficient (ICC)	0.56	-0.31	0.88	0.99	0.99	0.98

Repeatability of net CSF flow and CSF stroke volume (mean ± standard deviation (SD)). During expiration, inspiration, and no gating, showing the results for the first and second measurement, the average of the first and second measurement, and the difference (mean ± SD) and absolute difference (mean (range)) between the first and second measurement, and the intraclass correlation coefficient (ICC) between both measurements.

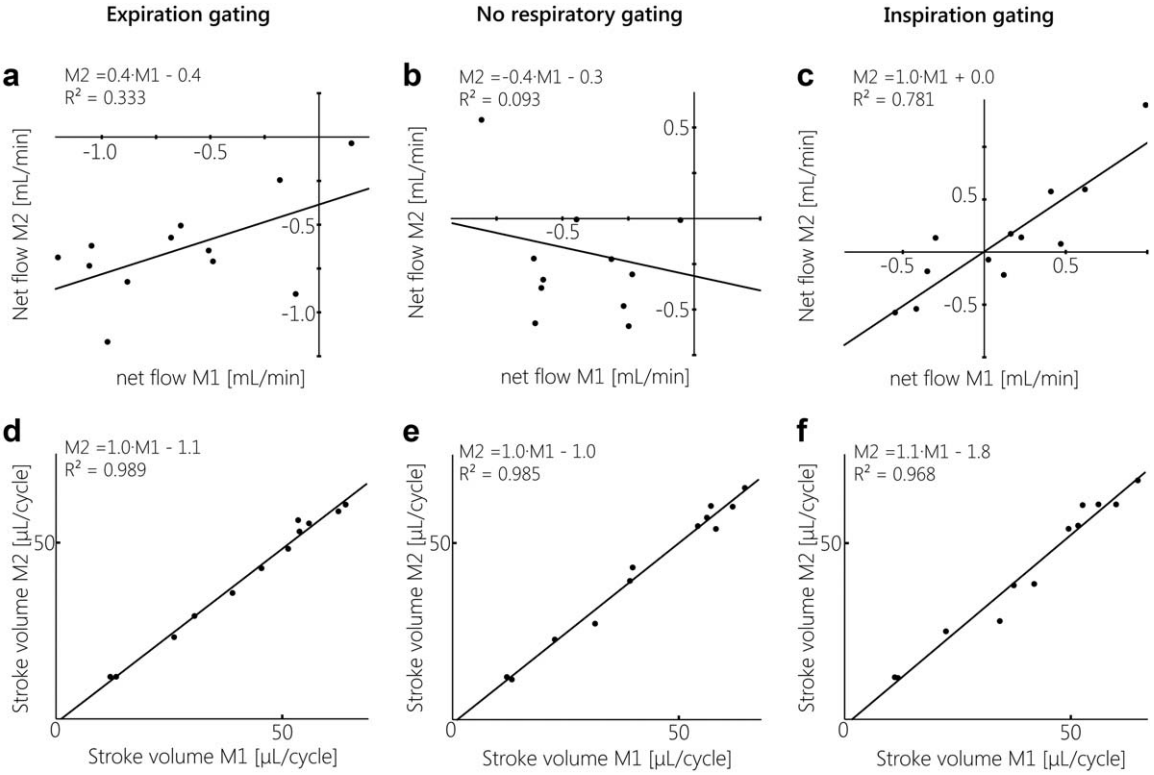

FIGURE 6: Linear regression analysis between the first (independent variable) and second (dependent variable) measurements for net CSF flow (A–C) and stroke volume (D–F), for gating on expiration, no respiratory gating, and gating on inspiration. For net CSF flow, only gating on inspiration showed very good repeatability, as the regression line was very close to M2 = M1; a fair correlation between both measurements was seen for gating on expiration, and no significant correlation was found between both measurements without respiratory gating. For stroke volume, repeatability was good for all respiratory conditions, with regression lines approximating M2 = M1.

the net CSF flow measurements was best during inspiration. A significant, positive association was found between CSF stroke volume and net CSF flow difference between inspiration and expiration gated measurements. During the measurements without respiratory gating two outliers were found in the repeated measurements of two different subjects with relatively large cranially directed net CSF flow.

The observed change in net CSF flow during inspiration compared with expiration is in line with the altered CSF dynamics measured using real-time PC-MRI measurements, as shown in the literature. Klose et al[15] qualitatively investigated CSF flow dynamics over the cardiac and respiratory cycle, and showed increased cranial flow and decreased caudal flow during inspiration, and the reversed

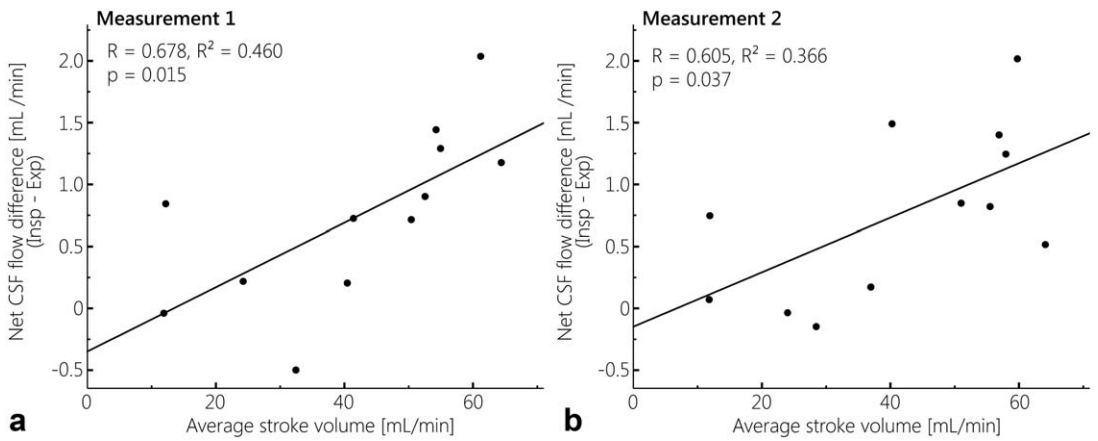

FIGURE 7: Regression analysis between the net CSF flow difference for inspiration minus expiration, and the average stroke volume for expiration and inspiration, for measurement 1 (A) and measurement 2 (B). Significant, positive associations were found for both measurements.

effect during expiration. Yamada et al[16] investigated CSF movement in the cerebral aqueduct during inspiration and expiration, and found cranial CSF motion during inspiration, and caudal CSF motion during expiration. Dreha-Kulaczewski et al[13,21] performed real-time measurements of CSF flow dynamics, and found upward (cranial) CSF flow during inspiration, and downward CSF flow during expiration. Chen et al[14] performed real-time velocity mapping, and also found cranial CSF velocities during inspiration, which was reversed during expiration. Takizawa et al[22] investigated the relative contributions of the cardiac and respiratory cycles to CSF velocity and CSF displacement, and showed that the contribution of the respiratory cycle to CSF velocity in the aqueduct is smaller compared with the cardiac cycle, but that the resulting total displacement through the aqueduct is larger than the displacements induced by the cardiac cycle. Daouk et al[23] investigated blood and CSF flows using signal intensity changes, and found that arterial blood flow is influenced mostly by the cardiac cycle, while venous blood flow is influenced mostly by the respiratory cycle. CSF appeared to act as a buffer between the arterial and venous blood compartments.

Real-time PC-MRI measurements could potentially be used to determine net CSF flow through the aqueduct, which is usually performed using PC-MRI, as in this work. At 3T, Dreha et al[21] achieved a temporal resolution of 135 msec for a pair of two flow-encoded images, and Yildiz et al[24] achieved a temporal resolution of 50 msec, which could offer net CSF flow measurements that are not confounded by the respiratory cycle. However, currently the application of real-time PC-MRI to measure net CSF flow is limited by the relatively low spatial resolution, Dreha et al[21] achieved a spatial resolution of $1.2 \times 1.2 \times 5$ mm^3, and Yildiz et al[24] achieved a spatial resolution of $2.5 \times 2.5 \times 10$ mm^3, making this technique more prone to partial volume. PC-MRI, on the other hand, offers much better spatial resolution, but low temporal resolution. Furthermore, it is important to evaluate if net CSF flow over one cardiac cycle, which can be acquired with real-time PC-MRI measurements, is representative for the net CSF flow over a longer period of time.

The average net CSF flow acquired without respiratory gating in this work (0.31 ± 0.18 mL/min) is in line with values found in the literature, ranging between 0.26–0.74 mL/min.[8,10–12,25–27] In these studies spatial resolutions varied between $0.39 \times 0.39 \times 6$ mm^3 and $0.9 \times 0.9 \times 6$ mm^3, scanning was performed at 1.5T or 3T, and 16 or 32 frames per cardiac cycle were acquired. Our net CSF flow values are on the lower end of this range, which was partially caused by the two outliers showing net cranial flow when no respiratory gating was used (excluding these two subjects would result in an average net CSF flow of 0.35 ± 0.16 mL/min). Furthermore, our spatial resolution was relatively high ($0.45 \times 0.45 \times 3$ mm^3), especially regarding slice thickness, reducing partial volume in the aqueduct ROI and thereby resulting in smaller overestimation of net CSF flow. Also, the relatively small slice thickness, short TR, and low flip angle used in this work limited the possible bias in the acquired CSF velocities induced by RF saturation.[28] Finally, a relatively high temporal resolution and SNR were achieved (scanning was performed at 7T, and 36–45 frames per cardiac cycle were acquired, with a temporal resolution of 48 msec), resulting in a relatively high accuracy of the estimated net CSF flow, which is small relative to the stroke volumes.

The stroke volumes found in this work (41 ± 18, 42 ± 19, and 42 ± 19 μL/cycle for gating on expiration, gating on inspiration, and no respiratory gating, respectively) are in line with values found in the literature, ranging between 30–50 μL/cycle.[4,29,30]

Net CSF flow measurements are influenced by the respiratory cycle. In this work, for two different subjects cranial net CSF flow was found when no respiratory gating was applied, which is likely due to a difference in the (changeable) respiration between these measurements. Also, in previous exploratory work[17] and in the literature[18] such outliers were found, with cranial net CSF flow in healthy subjects when no respiratory gating was performed. It is perhaps illustrative that the results without respiratory gating were significantly different from the inspiration gated (but not expiration gated) results in the first measurement, while this was the opposite in the second measurement (Table 1). This suggests that, when no respiratory gating is performed, net CSF flow may be closer to either inspiration or expiration, and respiration effects may not average out over the acquisition.

These results violate the general assumption that all respiratory variation averages out over the acquisition time of net CSF flow measurements.[10] Also, Yildiz et al[24] concluded that respiration effects average out in conventional PC-MRI, based on phantom measurements. However, Yildiz et al analyzed only the flow curve shape, but did not show the net flow. From figure 3 in the work by Yildiz et al, a slight shift between the velocity curves can be observed. Estimating the net flows from this figure using an online tool to digitize the plot[31] yields a net flow difference between the PC-MRI measurements with and without respiration effects of ~0.4 ml/min, which is comparable to the total net CSF flows in our in vivo measurements (data not shown).

We found that stroke volume was not affected by respiration, implying that the respiratory phase determines the offset of the CSF flow curve over the cardiac cycle, but does not alter the flow curve shape. The large influence of respiration on net CSF flow measurements may be explained by changes in thoracic pressure over the respiratory cycle.

During inspiration a drop in thoracic pressure occurs, resulting in increased outflow of venous blood from the head. During expiration the opposite happens: thoracic pressure increases, resulting in reduced outflow of venous blood from the head.[21] According to the Monro–Kellie hypothesis,[32] these changes in intracranial blood volume must be compensated by changes in CSF volume.

Between the CSF stroke volume and the net CSF flow difference between inspiration and expiration a significant correlation was found. Thus, in subjects with larger CSF flow pulsatility over the cardiac cycle, also larger respiratory-induced CSF flow variation was found. This suggests that either respiration or the cardiac cycle can be used as a non-invasive driver to assess the cerebrovascular compliance: both stroke volume and net CSF flow difference between inspiration and expiration reflect changes in intracranial blood volume variation over the cardiac and respiratory cycles. Interindividual differences in CSF dynamics in the aqueduct may either reflect differences in (intracranial) blood volume pulsation, or differences in the relative contributions of the ventricles and subarachnoidal space to accommodate blood volume pulsations. Following the Monro–Kellie hypothesis, CSF flow from either the ventricles (via the aqueduct) or the subarachnoidal space (via the spinal canal) can compensate for this blood volume variation. Balédent et al[33] showed that stroke volumes through the aqueduct are only ~10% of the stroke volumes through the spinal canal, without correlation between these two stroke volumes. Therefore, spinal CSF measurements should be included for studying the cerebrovascular compliance. Repeatability of the net flow measurements in this work is best for inspiration, followed by expiration. When no respiratory gating was performed the ICC was negative. Removing the two outliers (with cranial net CSF flow) would result in an ICC of 0.24. The low repeatability when no respiratory gating was performed is probably due to the influence of the respiratory cycle. Wåhlin et al[27] also investigated the repeatability of net CSF flow measurements without respiratory gating, and found low ICC. They suggested that this was caused by the relatively small aqueductal CSF flow with respect to the pulsatile CSF flow rates, and imperfect background correction. However, since no respiratory gating was performed, also respiratory effects may have contributed to this low ICC.

During inspiration we observed the highest intersubject variation. Relatively large intersubject differences can also be observed in the net CSF flow profiles in the aqueduct, for all respiratory conditions. The hydrodynamic theory by Greitz at al[30,34] states that stiffening of extracranial arterial vessel walls leads to larger expansion of intracerebral vessels over the cardiac cycle, thereby increasing CSF pulsatility. Furthermore, it has been shown that CSF pulsatility increases with age.[35] Possibly respiration-induced CSF pulsatility also varies between subjects, similar to cardiac-induced CSF pulsatility.

Small variations can be observed between the aqueduct ROIs during inspiration gating, expiration gating, and without respiratory gating. These small variations of the aqueduct area had only a minor (nonsignificant) impact on the acquired net CSF flow, as the velocities at the edges are very low (data not shown). This may be (partly) due to motion between the different scans. Also, variations in background noise between the scans may play a role, since the ROIs are selected by including all voxels with a signal intensity significantly higher than the noise floor.

During the respiration gated measurements a few outliers were observed. In one subject (Subject 3) cranial net flow was found during expiration, and caudal flow was found during inspiration. The recorded physiology (cardiac and respiration) did not show striking irregularities. In this subject an irregular shape of the aqueduct was observed, leading to local minor stenosis. The radiologist rated this as normal anatomical variation, but this may have led to non-laminar flow and, thus, to errors in the PC-MRI measurements. Furthermore, in two subjects similar (caudal) net CSF flows were observed during expiration and inspiration. In neither of these subjects were irregularities found in the anatomy or recorded physiology. It is uncertain to what extent these subjects indeed have less variability with respiration or whether unidentified measurement errors played a role.

There is currently a debate whether CSF is produced by the choroid plexus alone, but the main consensus is that CSF is produced mainly by the choroid plexus.[2,36–38] This work shows that net CSF flow measurements with PC-MRI are not necessarily suitable as a marker for CSF production in the lateral ventricles, because of the considerable confounding influence of the respiratory cycle on these measurements.

Cranially directed net CSF flows have been found in communicating hydrocephalus by Hladky et al.[37] However, Schroth and Klose[39] observed net caudal CSF flow over one cardiac cycle using real-time MRI measurements in normal pressure hydrocephalus patients, although the CSF pulsation was found to be of higher amplitude. Also, Gideon et al[40] found mostly caudal net CSF flows in normal-pressure hydrocephalus patients. It could be that the reported reversed (cranial) net CSF flows, acquired with PC-MRI, were affected by altered CSF dynamics with respect to the respiratory cycle. Our results indicate that the effect size of respiration on net CSF flow measurements is sufficiently large to find reversed (cranial) net CSF flow over the cardiac cycle (Fig. 4).

When respiration is taken into account, net CSF flow measurements may offer an interesting quantitative measure

for CSF dynamics, and may be used to study differences between the healthy and diseased brain.

The major limitation of this work is the limited number of subjects, which makes it difficult to interpret the outliers in the measurements without respiratory gating. Also, no clinical patients were included. Therefore, it remains unknown if respiration also confounds net CSF flow measurements in diseased populations. If an MRI method for net CSF flows could be developed without confounding effects from respiration, it should be developed for field strengths widely available in the clinic (1.5T or 3T), as 7T MRI is still not widely available.

Furthermore, since only aqueductal CSF flow was measured, it was not possible to identify whether interindividual differences in aqueductal CSF flow dynamics reflect differences in (intracranial) blood volume pulsation, or differences in the relative contributions of the ventricles and subarachnoidal space to compensate for blood volume pulsations. Therefore, in future work spinal measurements should be performed together with aqueductal CSF flow measurements.

Finally, no respiratory scheme was enforced. Therefore, a relatively large variation in respiratory patterns occurred, with deeper or more shallow breaths and faster or slower breaths, as compared with a fixed respiratory scheme, as used in the literature.[13,21] Regularizing the breathing patterns by providing the subjects with a paced breathing cue may improve the consistency of the net CSF flow measurements and, thus, the confounding effects of respiration. This has to be evaluated in the future, and its performance may still be variable between different subjects and between patient groups.

In conclusion, net CSF flow through the cerebral aqueduct was increased during expiration, and reversed (in cranial direction) during inspiration. When no respiratory gating was used, mostly caudal net CSF flow was found, except for two outliers. Repeatability was best for respiratory gating on inspiration, followed by gating on expiration. CSF stroke volume was not affected by respiration. A positive, significant association was found between stroke volume and net flow difference between inspiration and expiration. Since the measured net CSF flows are considerably confounded by the respiratory cycle, care should be taken in linking measured net CSF flows to CSF production.

Acknowledgments

Contract grant sponsor: European Research Council under the European Union's Seventh Framework Programme; contract grant numbers: FP7/2007-2013 / ERC grant agreement 337333 (SmallVesselMRI); Contract grant sponsor: European Union's Horizon 2020 Programme; contract grant numbers: H2020 / ERC grant agreement 637024 (HEARTOFSTROKE), 666881 (SVDs@target)

References

1. Jessen NA, Munk ASF, Lundgaard I, Nedergaard M. The glymphatic system: a beginner's guide. Neurochem Res 2015;40:2583–2599.
2. Spector R, Robert Snodgrass S, Johanson CE. A balanced view of the cerebrospinal fluid composition and functions: Focus on adult humans. Exp Neurol 2015;273:57–68.
3. May C, Kaye JA, Atack JR, Schapiro MB, Friedland RP, Rapoport SI. Cerebrospinal fluid production is reduced in healthy aging. Neurology 1990;40:500–503.
4. Stoquart-ElSankari S, Balédent O, Gondry-Jouet C, Makki M, Godefroy O, Meyer M-E. Aging effects on cerebral blood and cerebrospinal fluid flows. J Cereb Blood Flow Metab 2007;27:1563–1572.
5. Silverberg GD, Heit G, Huhn S, et al. The cerebrospinal fluid production rate is reduced in dementia of the Alzheimer's type. Neurology 2001;57:1763–1766.
6. de Leon MJ, Li Y, Okamura N, et al. CSF clearance in Alzheimer disease measured with dynamic PET. J Nucl Med 2017;1471–1476.
7. Bradley WG. CSF flow in the brain in the context of normal pressure hydrocephalus. AJNR Am J Neuroradiol 2015;36:831–838.
8. Feinberg DA, Mark AS. Human brain motion and cerebrospinal fluid circulation demonstrated with MR velocity imaging. Radiology 1987; 163:793–799.
9. Ståhlberg F, Mogelvang J, Thomsen C, et al. A method for MR quantification of flow velocities in blood and CSF using interleaved gradient-echo pulse sequences. Magn Reson Imaging 1989;7:655–667.
10. Enzmann DR, Pelc NJ. Cerebrospinal fluid flow measured by phase-contrast cine MR. AJNR Am J Neuroradiol 1993;14:1301–1307.
11. Balédent O, Gondry-Jouet C, Meyer ME, et al. Relationship between cerebrospinal fluid and blood dynamics in healthy volunteers and patients with communicating hydrocephalus. Invest Radiol 2004;39: 45–55.
12. Yoshida K, Takahashi H, Saijo M, et al. Phase-contrast MR studies of CSF flow rate in the cerebral aqueduct and cervical subarachnoid space with correlation-based segmentation. Magn Reson Med Sci 2009;8:91–100.
13. Dreha-Kulaczewski S, Joseph AA, Merboldt K-D, Ludwig H-C, Gärtner J, Frahm J. Inspiration is the major regulator of human CSF flow. J Neurosci 2015;35:2485–2491.
14. Chen L, Beckett A, Verma A, Feinberg DA. Dynamics of respiratory and cardiac CSF motion revealed with real-time simultaneous multislice EPI velocity phase contrast imaging. Neuroimage 2015;122:281–287.
15. Klose U, Strik C, Kiefer C, Grodd W. Detection of a relation between respiration and CSF pulsation with an echoplanar technique. J Magn Reson Imaging 2000;11:438–444.
16. Yamada S, Miyazaki M, Yamashita Y, et al. Influence of respiration on cerebrospinal fluid movement using magnetic resonance spin labeling. Fluids Barriers CNS 2013;10:36–42.
17. Spijkerman JM, Siero JCW, Geurts LJ, et al. Quantification of cerebrospinal fluid flow through the cerebral aqueduct using 7T MRI. In: Proc 25th Annual Meeting ISMRM, Honolulu; 2017. p 2849.
18. Nilsson C, Ståhlberg F, Thomsen C, Henriksen O, Herning M, Owman C. Circadian variation in human cerebrospinal fluid production measured by magnetic resonance imaging. Am J Physiol 1992;262:R20–R24.
19. Bouvy WH, Geurts LJ, Kuijf HJ, et al. Assessment of blood flow velocity and pulsatility in cerebral perforating arteries with 7-T quantitative flow MRI. NMR Biomed 2016;9:1295–1304.

20. Goldstein RM, Zebker HA, Werner CL. Satellite radar interferometry: two–dimensional phase unwrapping. Radiol Sci 1988:713-720.
21. Dreha-Kulaczewski S, Joseph AA, Merboldt K-D, Ludwig H-C, Gärtner J, Frahm J. Identification of the upward movement of human CSF in vivo and its relation to the brain venous system. J Neurosci 2017;37: 2395–2402.
22. Takizawa K, Matsumae M, Sunohara S, Yatsushiro S, Kuroda K. Characterization of cardiac and respiratory-driven cerebrospinal fluid motion based on asynchronous phase-contrast magnetic resonance imaging in volunteers. Fluids Barriers CNS 2017;14:1–8.
23. Daouk J, Bouzerar R, Baledent O. Heart rate and respiration influence on macroscopic blood and CSF flows. Acta Radiol 2017;58:977–982.
24. Yildiz S, Thyagaraj S, Jin N, et al. Quantifying the influence of respiration and cardiac pulsations on cerebrospinal fluid dynamics using real-time phase-contrast MRI. J Magn Reson Imaging 2017;46:431–439.
25. Huang T-Y, Chung H, Chen M, et al. Supratentorial cerebrospinal fluid production rate in healthy adults: quantification with two-dimensional cine phase-contrast MR imaging with high temporal and spatial resolution. Radiology 2004;233:603–608.
26. Piechnik SK, Summers PE, Jezzard P, Byrne JV. Magnetic resonance measurement of blood and CSF flow rates with phase contrast — Normal values, repeatability and CO2 reactivity. Acta Neurochir Suppl 2008;263–270.
27. Wåhlin A, Ambarki K, Hauksson J, Birgander R, Malm J, Eklund A. Phase contrast MRI quantification of pulsatile volumes of brain arteries, veins, and cerebrospinal fluids compartments: Repeatability and physiological interactions. J Magn Reson Imaging 2012;35:1055–1062.
28. Ragunathan S, Pipe JG. Radiofrequency saturation induced bias in aqueductal cerebrospinal fluid flow quantification obtained using two-dimensional cine phase contrast magnetic resonance imaging. Magn Reson Med 2018;79:2067–2076.
29. Kim DS, Choi JU, Huh R, Yun PH, Kim DI. Quantitative assessment of cerebrospinal fluid hydrodynamics using a phase-contrast cine MR image in hydrocephalus. Child's Nerv Syst 1999;15:461–467.
30. Bateman GA, Levi CR, Schofield P, Wang Y, Lovett EC. The pathophysiology of the aqueduct stroke volume in normal pressure hydrocephalus: Can co-morbidity with other forms of dementia be excluded? Neuroradiology 2005;47:741–748.
31. WebPlotDigitizer [https://automeris.io/WebPlotDigitizer/]
32. Mokri B. The Monro-Kellie hypothesis. Neurology 2001;56:1746–1748.
33. Balédent O, Henry-Feugeas M-CC, Idy-Peretti I. Cerebrospinal fluid dynamics and relation with blood flow. Invest Radiol 2001;36:368–377.
34. Greitz D, Hannerz J, Rahn T, Bolander H, Ericsson A. MR imaging of cerebrospinal fluid dynamics in health and disease on the vascular pathogenesis of communicating hydrocephalus and benign intracranial hypertension. Acta Radiol 1994;35:204–211.
35. Beggs CB, Magnano C, Shepherd SJ, et al. Aqueductal cerebrospinal fluid pulsatility in healthy individuals is affected by impaired cerebral venous outflow. J Magn Reson Imaging 2014;40:1215–1222.
36. Orešković D, Radoš M, Klarica M. Role of choroid plexus in cerebrospinal fluid hydrodynamics. Neuroscience 2017;354:69–86.
37. Hladky SB, Barrand MA. Mechanisms of fluid movement into, through and out of the brain: evaluation of the evidence. Fluids Barriers CNS 2014;11:26–57.
38. Hladky SB, Barrand MA. Fluid and ion transfer across the blood-brain and blood-cerebrospinal fluid barriers; a comparative account of mechanisms and roles. Fluids Barriers CNS 2016;13:19–87.
39. Schroth G, Klose U. Cerebrospinal fluid flow III. Pathological cerebrospinal fluid pulsations. Neuroradiology 1992;35:16–24.
40. Gideon P, Ståhlberg F, Thomsen C, Gjerris F, Sørensen PS, Henriksen O. Cerebrospinal fluid flow and production in patients with normal pressure hydrocephalus studied by MRI. Neuroradiology 1994;36:210–215.